Analytical modeling of dual-junction tandem solar cells based on an InGaP/GaAs heterojunction stacked on a Ge substrate

F. Bouzid[1,*], F. Pezzimenti[2], L. Dehimi[1,3], F.G. Della Corte[2], M. Hadjab[1], and A. Hadj Larbi[1]

[1]Thin Films Development and Applications Unit UDCMA, Setif / Research Center in Industrial Technologies CRTI, P.O. Box 64, Cheraga 16014, Algiers, Algeria.

[2]DIIES – Mediterranea University of Reggio Calabria, 89122 Reggio Calabria, Italy.

[3]Faculty of Science, University of Batna, Batna 05000, Algeria.

[*]E-mail address: f.bouzid@crti.dz

Abstract- An analytical model is used to describe the elctrical characteristics of a dual-junction tandem solar cell performing a conversion efficiency of 32.56% under air mass 1.5 global (AM1.5G) spectrum. The tandem structure consists of a thin heterojunction top cell made of indium gallium phosphide (*InGaP*) on gallium arsenide (*GaAs*), mechanically stacked on a relatively thick germanium (*Ge*) substrate which acts as bottom cell. In order to obtain the best performance of such a structure, we simulate for both the upper and lower sub-cell the current density-voltage, power density-voltage, and spectral response behaviours taking into account the doping-dependent transport parameters and a wide range of minority carrier surface recombination velocities.

For the proposed tandem cell, our calculations predict that optimal photovoltaic (PV) parameters, namely the short-circuit current density (J_{sc}), open-circuit voltage (V_{oc}), maximum power density (P_{max}), and fill factor (FF) are J_{sc} = 28.25 mA/cm^2, V_{oc} = 1.24 V, P_{max} = 31.64 mW/cm^2, and FF = 89.95%, respectively. The present study could turn useful to support the design of high efficiency dual junction structures by investigating the role of different materials and physical parameters.

Keywords- Analytical modeling, tandem solar cell, spectral response, conversion efficiency.

This is a post-peer-review, pre-copyedit version of an article published in Journal of Electronic Materials, n. 48, pp. 4107-4116, 2019. The final authenticated version is available online at: https://doi.org/10.1007/s11664-019-07180-z

Introduction

The major research challenges in photovoltaic systems are to increase the conversion efficiency and make the devices more cost effective. With these purposes, several designs of solar cells have been presented in literature mainly based on the use of different semiconductors in multi-junction tandem structures, both monolithically grown and mechanically stacked, where the material bandgap energy (E_g) decreases in the depth direction from the top surface [1-7]. However, there are some technological issues associated with the multi-junction configurations. In particular, the monolithic design suffers the crystal lattice mismatch and the need to match the current produced in each junction layer. These issues prevent the monolithic stack to reach its theoretical efficiency and became critical as the effective number of junctions increases. On the other hand, the mechanical stacked approach circumvents the above-mentioned drawbacks but it presents an additional complexity related to the use of one or more optically transparent and electrically conductive adhesive layers for mechanically stacking the different solar cells. In more detail, each sub-junction can be fabricated separately on its own substrate and then combined in a multi-junction structure that will be less sensitive to spectral variations if compared with the monolithic counterpart. Moreover, in principle, in a mechanically stacked solar cell each junction can be connected separately allowing the extraction of the total amount of current for higher power yields.

Multi-junction solar cells based on group III-V semiconductors have been worldwide recognized as optimal structures for achieving a high photovoltaic conversion efficiency. Recent records of commercial and laboratory state-of-the-art devices are summarized in Ref. 8. In particular, indium gallium phosphide (*InGaP*), with an E_g of 1.86-1.9 eV, and gallium arsenide (*GaAs*), with an E_g of 1.42-1.435 eV, are considered suitable materials for the production of thin film heterojunction structures where the *InGaP* layer absorbs mainly the visible part of the incident solar spectrum while the infrared part is mostly absorbed by the

GaAs layer [9-15]. In addition, when the $In_{1-x}Ga_xP$ alloy has a *Ga* composition ratio of 0.51, the $In_{0.49}Ga_{0.51}P$ ternary compound can be grown on a *GaAs* layer with an appropriate lattice match as investigated experimentally in Ref. 10 and references therein. Earlier studies have also shown that germanium (*Ge*) can be used as starting substrate (i.e., bottom cell) in high efficiency multi-junction solar cells [16-19], owing to its low bandgap ($E_g \cong 0.66$ eV) which allows a good response at the longer wavelengths (> 900 nm).

Nowadays, in order to overcome the difficulties encountered during the experimental optimization of existing devices, or the design of novel structures, the deployment of intensive modeling efforts plays a key role. To this extent, in this study we have investigated the possibility to obtain a conversion efficiency in excess of 32.5% for a dual-junction tandem configuration using an analytical model developed to evaluate the performance of both homojunction and heterojunction single solar cells as well as multi-junction stacked structures. In particular, we have adopted a spectral irradiance consistent with the air mass 1.5 global (AM1.5G) data that refer to the American Society for Testing and Materials (ASTM) G-173 standard. By calculating the spectral irradiance numerical integral in the 300-2050 nm wavelength range, the assumed incident power density was 971.5 W/m^2.

In more detail, we have designed and simulated a dual-junction tandem solar cell based on a thin $In_{0.49}Ga_{0.51}P/GaAs$ heterojunction top cell stacked on a *Ge* bottom cell. The current density-voltage $J(V)$, power density-voltage $P(V)$, and spectral response $SR(\lambda)$ behaviors of the individual sub-cells have been evaluated at first. Then, we have extracted the main photovoltaic parameters which determine the performance of the tandem in terms of short-circuit current density (J_{sc}), open-circuit voltage (V_{oc}), maximum power density (P_{max}), fill factor (FF), and conversion efficiency (η). Different values of fundamental physical parameters, such as the doping concentration and minority carrier surface recombination velocity in the two sub-cell emitters, have been taken into account during the simulations.

1. Cell structure

The considered $In_{0.49}Ga_{0.51}P/GaAs/Ge$ dual-junction tandem solar cell is schematized in Fig. 1 (plot not to scale). The $In_{0.49}Ga_{0.51}P/GaAs$ heterojunction top cell is stacked on a relatively thick *Ge* substrate acting as bottom cell by means of a transparent adhesive thin film that needs to be conductive. The assumed cell surface area is 1 cm^2.

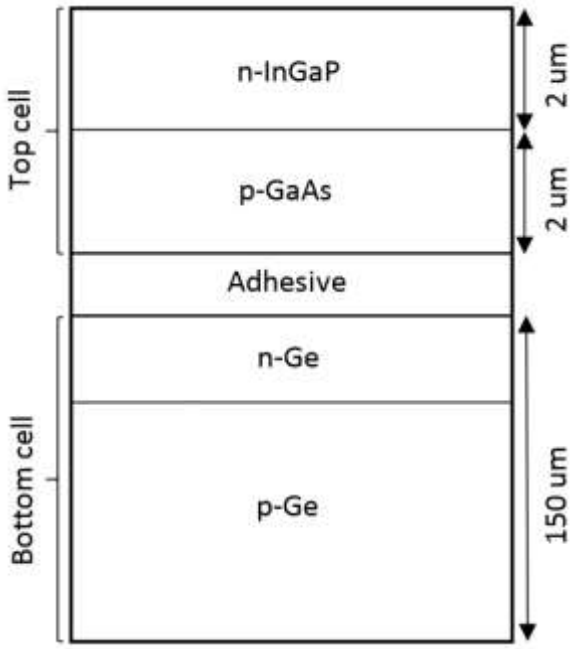

Fig.1. Simulated $In_{0.49}Ga_{0.51}P/GaAs/Ge$ dual-junction tandem solar cell (2-terminal device).

By passing through the three layers with different bandgaps, each layer absorbs a part of the incident spectrum. Optical losses due to grid shadowing and reflection from each semiconductor surface have been neglected, since they are strictly dependent on the metal contact design and the use of optimized antireflection coating layers. For the sake of simplicity, explicit effects due to the presence of the adhesive film have also been neglected. In fact, a high optical transparency for permanent bonding adhesives in mechanically stacked solar cells, except for very short wavelengths, has already been demonstrated [6,20,21]. Finally, similarly to other theoretical works [22,23], the solar cell *J-V* characteristics have been calculated using

the single diode model with an ideality factor of 1 and no series or shunt resistance losses considered.

2. Model description

3.1 Theoretical basis

The total amount of current density (J_{Total}) of a solar cell under illumination that can be measured on an external load resistor is [24]

$$J_{Total} = J_L - J_D \,, \tag{1}$$

where J_L is the current density generated by the incident light assuming that each incident photon with an energy greater than the material bandgap gives origin to an electron-hole pair, and J_D is the current density in absence of illumination (in dark) for a given bias voltage.

The component J_L is strongly dependent on the material optical properties and it represents the sum of the photocurrents generated in the three fundamental regions of a cell, namely emitter, depleted region, and base. A typical expression of J_L is in the form of

$$J_L = \int_{\lambda_{\min}}^{\lambda_{\max}} q \times F(\lambda) \times SR(\lambda) d\lambda \,, \tag{2}$$

where q is the electron charge, F is the incident illumination flux, λ is the wavelength of an incident photon, λ_{min} is the minimum wavelength absorbed by each layer, and λ_{max} is the cut-off wavelength depending on the material bandgap energy, E_g, as follows:

$$\lambda_{\max} = \frac{h \times c}{E_g} \,. \tag{3}$$

Here, h is Planck's constant, and c is the speed of light. Finally, $SR(\lambda)$ is the spectral response considered as a sum of three different contributions, i.e.

$$SR(\lambda) = SR_{Emitter}(\lambda) + SR_{Depleted\,reg.}(\lambda) + SR_{Base}(\lambda). \tag{4}$$

The $SR(\lambda)$ of a solar cell describes its ability to convert photons of different wavelengths into electric current. For the $In_{0.49}Ga_{0.51}P/GaAs$ top cell, we can write:

$$SR_{Emitter} = \left[\frac{q(1-R_0)\alpha_{\mathrm{InGaP}} L_p}{\alpha_{\mathrm{InGaP}}{}^2 L_p^2 - 1} \right] \times \left[\frac{\left(\frac{S_p L_p}{D_p} + \alpha_{\mathrm{InGaP}} L_p \right) - e^{-\alpha_{\mathrm{InGaP}} y_1} \left(\frac{S_p L_p}{D_p} \cosh \frac{y_1}{L_p} + \sinh \frac{y_1}{L_p} \right)}{\left(\frac{S_p L_p}{D_p} \sinh \frac{y_1}{L_p} + \cosh \frac{y_1}{L_p} \right)} - \alpha_{\mathrm{InGaP}} L_p e^{-\alpha_{\mathrm{InGaP}} y_1} \right], \quad (5)$$

$$SR_{Base} = \left[\frac{q(1-R_3)\alpha_{GaAs} L_n}{\alpha_{GaAs}{}^2 L_n^2 - 1} \right] \times e^{-\alpha_{GaAs} y_3} \times \left[\alpha_{GaAs} L_n - \frac{\frac{S_n L_n}{D_n} \left(\cosh \frac{y_4 - y_3}{L_n} - e^{-\alpha_{GaAs}(y_4 - y_3)} \right) + \sinh \frac{y_4 - y_3}{L_n} + \alpha_{GaAs} L_n \exp\left(-\alpha_{GaAs}(y_4 - y_3)\right)}{\left(\frac{S_n L_n}{D_n} \sinh \frac{y_4 - y_3}{L_n} + \cosh \frac{y_4 - y_3}{L_n} \right)} \right], \quad (6)$$

$$SR_{Depleted\ reg.} = q\left(1 - R_0\right)\left(e^{-\alpha_{InGaP} y_1} - e^{-\alpha_{InGaP} y_2} - e^{-\alpha_{GaAs}(y_3 - y_2)} \right), \quad (7)$$

where y_1 is the distance from the *InGaP* surface to the beginning of the depleted region, y_2 is the thickness of the *InGaP* layer, y_3 is the edge of depleted region in the *GaAs* layer, y_4 is the total thickness of the top cell, R_0 is the reflected fraction of incident photons at the *InGaP* surface, R_3 is the reflected fraction of incident photons at the depletion edge y_3, S_p and S_n are the minority carrier surface recombination velocities, and L_p and L_n are the diffusion lengths for holes and electrons in the *InGaP* and *GaAs* layer, respectively. The diffusion lengths can be calculated according to the usual expression

$$L_{p,n} = \sqrt{D_{p,n} \times \tau_{p,n}} \ . \quad (8)$$

Here, $\tau_{p,n}$ are the minority carrier lifetimes, and $D_{p,n}$ are the carrier diffusion constants calculated by Einstein's relation

$$D_{p,n} = \frac{kT}{q} \mu_{p,n}, \quad (9)$$

where k is Boltzmann's constant, $\mu_{p,n}$ are the carrier mobilities, and T is the temperature.

Finally, in (5)-(7), α_{InGaP} and α_{GaAs} are the optical absorption coefficients of the *InGaP* and *GaAs* layers.

In the same way, for the *Ge* bottom cell we can write:

$$SR_{Emitter} = \left[\frac{q(1-R_0^{'})\alpha_{\mathrm{Ge}} L_p}{\alpha_{\mathrm{Ge}}{}^2 L_p^2 - 1} \right] \times \left[\frac{\left(\frac{S_p L_p}{D_p} + \alpha_{\mathrm{Ge}} L_p \right) - e^{-\alpha_{\mathrm{Ge}} y_1^{'}} \left(\frac{S_p L_p}{D_p} \cosh \frac{y_1^{'}}{L_p} + \sinh \frac{y_1^{'}}{L_p} \right)}{\left(\frac{S_h L_h}{D_h} \sinh \frac{x_1^{'}}{L_h} + \cosh \frac{x_1^{'}}{L_h} \right)} - \alpha_{\mathrm{Ge}} L_p e^{-\alpha_{\mathrm{Ge}} y_1^{'}} \right], \tag{10}$$

$$SR_{Base} = \left[\frac{q(1-R_3^{'})\alpha_{Ge} L_n}{\alpha_{Ge}{}^2 L_n^2 - 1} \right] \times e^{-\alpha_{Ge} y_3^{'}} \times \left[\alpha_{Ge} L_n - \frac{\frac{S_n L_n}{D_n} \left(\cosh \frac{y_4^{'} - y_3^{'}}{L_n} - e^{-\alpha_{Ge}\left(y_4^{'} - y_3^{'}\right)} \right) + \sinh \frac{y_4^{'} - y_3^{'}}{L_n} + \alpha_{Ge} L_n \exp\left(-\alpha_{Ge}\left(y_4^{'} - y_3^{'}\right)\right)}{\left(\frac{S_n L_n}{D_n} \sinh \frac{y_4^{'} - y_3^{'}}{L_n} + \cosh \frac{y_4^{'} - y_3^{'}}{L_n} \right)} \right], \tag{11}$$

$$SR_{Depleted\ reg.} = q\left(1 - R_0^{'}\right) \times e^{-\alpha_{Ge} y_1^{'}} \times \left(1 - e^{-\alpha_{Ge}\left(y_3^{'} - y_1^{'}\right)}\right), \tag{12}$$

where α_{Ge} is the optical absorption coefficient of the *Ge* layer.

The current density in absence of illumination, J_D, is described by the well-known Shockley's diode equation

$$J_D = J_0 \left[e^{\frac{qV}{kT}} - 1 \right], \tag{13}$$

where J_0 is the reverse saturation current for the top and bottom sub-cells in the form of

$$J_{0,Top} = \frac{qD_n n_i^2}{L_n N_a} \times \frac{\frac{S_n L_n}{D_n} \cosh(\frac{y_4}{L_n}) + \sinh(\frac{y_4}{L_n})}{\frac{S_n L_n}{D_n} \sinh(\frac{y_4}{L_n}) + \cosh(\frac{y_4}{L_n})} + \frac{qD_p n_i^2}{L_n N_d} \times \frac{\frac{S_p L_p}{D_p} \cosh(\frac{y_1}{L_p}) + \sinh(\frac{y_1}{L_p})}{\frac{S_p L_p}{D_p} \sinh(\frac{y_1}{L_p}) + \cosh(\frac{y_1}{L_p})}, \tag{14}$$

$$J_{0,Bottom} = \frac{qD_n n_i^2}{L_n N_a} \times \frac{\frac{S_n L_n}{D_n}\cosh(\frac{y'_4}{L_n}) + \sinh(\frac{y'_4}{L_n})}{\frac{S_n L_n}{D_n}\sinh(\frac{y'_4}{L_n}) + \cosh(\frac{y'_4}{L_n})} + \frac{qD_p n_i^2}{L_p N_d} \times \frac{\frac{S_p L_p}{D_p}\cosh(\frac{y'_1}{L_p}) + \sinh(\frac{y'_1}{L_p})}{\frac{S_p L_p}{D_p}\sinh(\frac{y'_1}{L_p}) + \cosh(\frac{y'_1}{L_p})} . \quad (15)$$

Here, N_a and N_d are the acceptor and donor concentrations, and n_i is the intrinsic carrier concentration depending on E_g as follows:

$$n_i = \sqrt{N_c N_v}\, e^{-\frac{E_g}{2kT}} , \quad (16)$$

where N_c and N_v are the carrier densities of states in the conduction and valence band, respectively.

3.2 Doping dependence of physical parameters

3.2.1 Bandgap narrowing

The material bandgap narrowing effect is modeled using the standard expression [25-27]

$$\Delta E_g = A\left(\frac{N}{10^{18}}\right)^{1/3} + B\left(\frac{N}{10^{18}}\right)^{1/4} + C\left(\frac{N}{10^{18}}\right)^{1/2} , \quad (17)$$

where the appropriate constants A, B, and C for the different device regions in Fig. 1 are listed in Table I [28,29].

Table I. Parameters for calculation of the material bandgap narrowing effect in meV.

	InGaP (n-type)	*GaAs* (p-type)	*Ge* (n-type)	*Ge* (p-type)
A	18	9.71	8.67	8.21
B	9.04	12.19	8.14	9.18
C	93.46	3.88	4.31	5.77

Moreover, the dependence of the $In_{1-x}Ga_xP$ bandgap energy on the *Ga* composition ratio is assumed in the form [30]

$$E_g(x) = -0.2722x^2 + 1.1925x + 1.3399 . \quad (18)$$

3.2.2 Carrier mobility

In order to describe the doping dependence of the carrier mobility, we used in the $In_{0.49}Ga_{0.51}P$ region a low field mobility model [31-33] based on Caughey and Thomas expression at $T = 300$ K, i.e.

$$\mu_{n,p} = \mu_{0n,p}^{\min} + \frac{\mu_{0n,p}^{\max} - \mu_{0n,p}^{\min}}{1 + \left(\frac{N}{N_{n,p}^{crit}} \right)^{\delta_{n,p}}} \quad , \tag{19}$$

where N is the local (total) doping concentration and $\mu_{0n,p}^{\min}$, $\mu_{0n,p}^{\max}$, $N_{n,p}^{crit}$, and $\delta_{n,p}$ are the reference parameters summarized in Table II [34]. Here, the carrier mobility parameters assumed for the *GaAs* and *Ge* regions are also reported referring to a simplified version of (19) with a unique reference value $\mu_{0n,p}$ (i.e, $\mu_{0n,p}^{\max} = \mu_{0n,p}$, and $\mu_{0n,p}^{\min} = 0$) at room temperature [28].

Table II. Carrier mobility parameters.

	$In_{0.49}Ga_{0.51}P$	*GaAs*	*Ge*
$\mu_{0n,p}^{\min}$ (cm^2/V·s)	400, 15	0	0
$\mu_{0n,p}^{\max}$ (cm^2/V·s)	4300, 150	9400, 400	3900, 2370
$N_{n,p}^{crit}$ (cm^{-3})	2×10^{16}, 1.5×10^{17}	1×10^{17}, 1.6×10^{18}	1×10^{17}, 1.2×10^{17}
$\delta_{n,p}$	0.7, 0.8	0.5, 1	0.5, 0.5

3.2.3 Carrier lifetime

The effective carrier lifetimes in the *InGaP* and *GaAs* regions were calculated at $T = 300$ K through the expression [35]

$$\frac{1}{\tau_{n,p}} = \frac{1}{\tau_{NRn,p}} + \beta_R \times N, \tag{20}$$

where β_R is the radiative recombination coefficient (average value), and $\tau_{NRn,p}$ are the non-radiative lifetimes given by

$$\frac{1}{\tau_{NRn,p}} = \frac{1}{\tau_{0n,p}} + C_{n,p} \times N^2 . \tag{21}$$

Here, $\tau_{0n,p}$ are the Shockley-Read-Hall lifetimes and $C_{n,p}$ are the Auger coefficients.

Finally, the electron and hole lifetimes in the *Ge* region were modeled using the standard expression [36]

$$\tau_{n,p} = \frac{\tau_{0n,p}}{1 + \left(\frac{N}{N_{n,p}^{ref}} \right)^{\vartheta_{n,p}}} . \tag{22}$$

The reference parameters assumed during the calculations are listed in Table III.

Table III. Carrier lifetime parameters.

	$In_{0.49}Ga_{0.51}P$	*GaAs*	*Ge*
β_R (cm^3/s)	(1±0.3)×10^{-10}	1.36×10^{-10}	-
$C_{n,p}$ (cm^6/s)	3×10^{-30}	5×10^{-31}	-
$\tau_{0n,p}$ (μs)	5	0.9	60, 47.4
$N_{n,p}^{ref}$ (cm^{-3})	-	-	6.7×10^{16}, 1.5×10^{17}
$\vartheta_{n,p}$	-	-	1.76, 1.545

Recent author papers addressed to the modeling of different photovoltaic devices support the presented simulation setup [37-43].

3. Photovoltaic parameters

When we assume J_{Total} = 0 in (1), the solar cell open-circuit voltage (V_{oc}) is a typical measure of the total charge-carrier recombination rate. This voltage mainly depends on the photo-generated current density as well as saturation current density, and can be calculated using [24]

$$V_{oc} = \frac{kT}{q} \times \ln\left(\frac{J_L}{J_0} + 1\right), \tag{23}$$

where in a multi-junction structure V_{oc} is the sum of the contributions of the individual sub-cells.

On the other hand, when the cell contacts are short-circuited we can calculate the short-circuit current density (J_{sc}), which is strictly dependent on the incident flux of photons resulting $J_{sc} \cong J_L$ in high-quality photovoltaic modules.

Considering the output power behavior of the cell ($P = J_{Total} \times V$), and in particular the maximum power point (MPP) when $dP/dV = 0$, the solar cell fill factor (FF) is defined by the following ratio:

$$FF = \frac{J_{MPP} \times V_{MPP}}{J_{sc} \times V_{oc}} , \tag{24}$$

where J_{MPP} and V_{MPP} are the current density and voltage values at the MPP of the $J_{Total}(V)$ curve, respectively.

Finally, the ratio between the maximum output power (P_{MPP}) and the incident radiation power (P_{Inc}) represents the solar cell overall conversion efficiency [24], i.e.

$$\eta = \frac{P_{MPP}}{P_{Inc}} = \frac{J_{MPP} \times V_{MPP}}{P_{Inc}} = \frac{FF \times J_{sc} \times V_{oc}}{P_{Inc}} . \tag{25}$$

4. Results and discussion

5.1 Performance analysis of the $In_{0.49}Ga_{0.51}P/GaAs$ top cell

The fundamental geometrical and physical parameters used in (5)-(7) for the simulation of the $In_{0.49}Ga_{0.51}P/GaAs$ top cell are listed in Table IV. In particular, in order to determine the best performance, wide ranges of both donor doping concentration (N_d) and minority carrier

surface recombination velocity (S_p) [44,45] are considered in the $In_{0.49}Ga_{0.51}P$ emitter fixing the parameters in the *GaAs* base.

Table IV. Physical and geometrical parameters for the $In_{0.49}Ga_{0.51}P/GaAs$ solar cell.

	$In_{0.49}Ga_{0.51}P$	*GaAs*
y_1 (μm)	0.1	-
y_2 (μm)	2	-
y_4 - y_2 (μm)	-	2
N_d (cm^{-3})	5×10^{13}-1×10^{18}	-
N_a (cm^{-3})	-	5×10^{18}
S_p (cm/s)	5×10^{3}-5×10^{4}	-
S_n (cm/s)	-	1×10^{5}

Note that, the total thickness y_4 in (6) is 4 μm, and the depletion region edge in the GaAs layer, i.e. y_3 in (6) and (7), is a value depending on the doping and bias level.

The conversion efficiency of the cell as a function of both N_d and S_p is shown in Fig. 2.

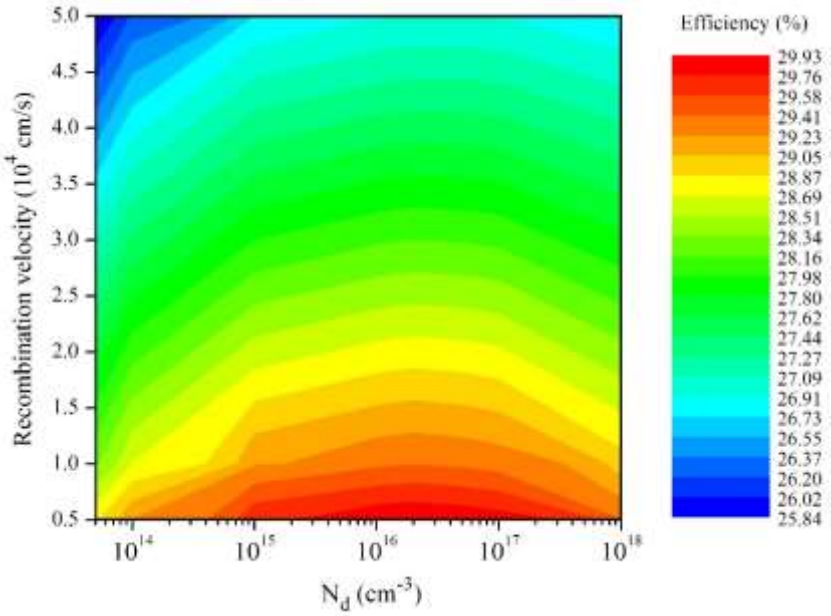

Fig. 2. Conversion efficiency of the $In_{0.49}Ga_{0.51}P/GaAs$ top cell as a function of N_d and S_p at T = 300 K.

As can be seen, by assuming an incident power density of 971.5 W/m^2 in the 300-2050 nm wavelength range, the cell conversion efficiency $\eta_{300-2050}$ reaches a peak of 29.93% for a donor

concentration of 2×10^{16} cm^{-3} and a hole recombination velocity of 5×10^{3} cm/s which is the lower limit that we have assumed. Afterward, this percentage tends to decrease for different values of N_d and, as expected, it decreases with increasing S_p. The minimum $\eta_{300-2050}$ value is 25.84% for $N_d = 5\times10^{13}$ cm^{-3}and $S_p = 5\times10^{4}$ cm/s.

From the theory, an increasing donor concentration leads to a decrease of the saturation current density J_0 (14). On the other hand, the increase of N_d leads to an increase of the open-circuit voltage V_{oc} and also a higher concentration of photo-generated carriers which determines a slight increase of J_{sc} as shown in Fig. 3.

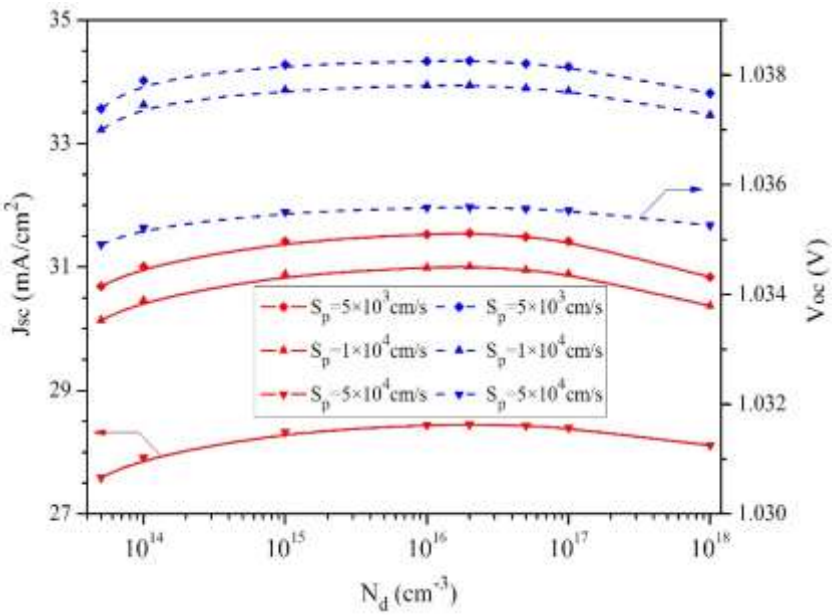

Fig. 3. J_{sc} and V_{oc} behaviors as a function of N_d and S_p for the $In_{0.49}Ga_{0.51}P/GaAs$ top cell.

However, as seen from this figure, the high doping effects have to be considered once the emitter doping concentration exceeds 2×10^{16} cm^{-3}. In fact, higher values of N_d determine a change in the device physics in terms of both minority carrier mobility (19) and carrier lifetime (20), which causes a decrease of the diffusion lengths and a decrease of J_{sc} consequently. At the same time, high doping levels increasingly determine an effect of apparent bandgap narrowing which causes an increase of the intrinsic carrier concentration (16) with an overall

increase of J_0 (14) and consequently a decrease of V_{oc} (23). Therefore, from Fig. 3 we can assume that the conversion efficiency of the top cell starts to decrease gradually for $N_d > 2\times10^{16}$ cm^{-3}. In addition, in accordance with Fig. 2, a decrease of the conversion efficiency is expected for increasing values of S_p. In fact, the photocurrent undergoes a reduction due to a lower probability of the photo-generated charges to reach the cell electrodes.

The spectral response of the $In_{0.49}Ga_{0.51}P/GaAs$ top cell for $N_d = 2\times10^{16}$ cm^{-3} and $S_p = 5\times10^3$ cm/s in the $In_{0.49}Ga_{0.51}P$ emitter, and $N_a = 5\times10^{18}$ cm^{-3} and $S_n = 1\times10^5$ cm/s in the *GaAs* base, is shown in Fig. 4.

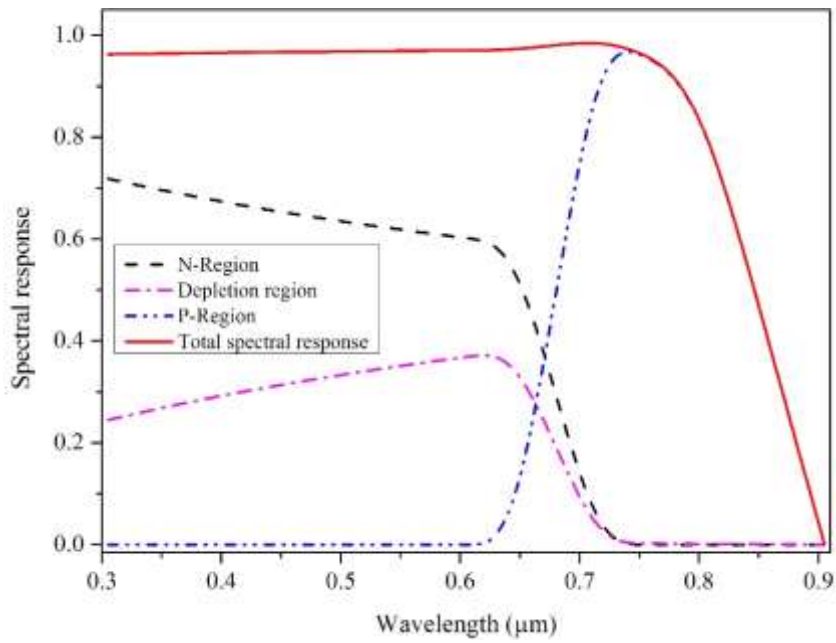

Fig. 4. Spectral response of the $In_{0.49}Ga_{0.51}P/GaAs$ top cell under AM1.5G spectrum.

During the simulations that involve the bandgap narrowing effect (17), we predict $E_{g(InGaP)} = 1.85$ eV and $E_{g(GaAs)} = 1.37$ eV. These energy values correspond to a cut-off wavelength (3) close to 0.67 μm for the N-region and 0.9 μm for the P-region, respectively. In other words, from the theory, the emitter absorbs all wavelengths for $\lambda < 0.7$ μm whereas the base absorbs all wavelengths for $0.7 \leq \lambda \leq 0.9$ μm. The resulting spectral response in Fig. 4 is higher than 0.95 for a large part of the considered incident spectrum.

Finally, by extracting the PV parameters from the $J(V)$ and $P(V)$ characteristics plotted in Fig. 5, we calculate J_{sc} = 31.55 mA/cm^2, V_{oc} = 1.04 V, P_{max} = 29.38 mW/cm^2, FF = 89.53% and $\eta_{300-2050}$ = 30.24%.

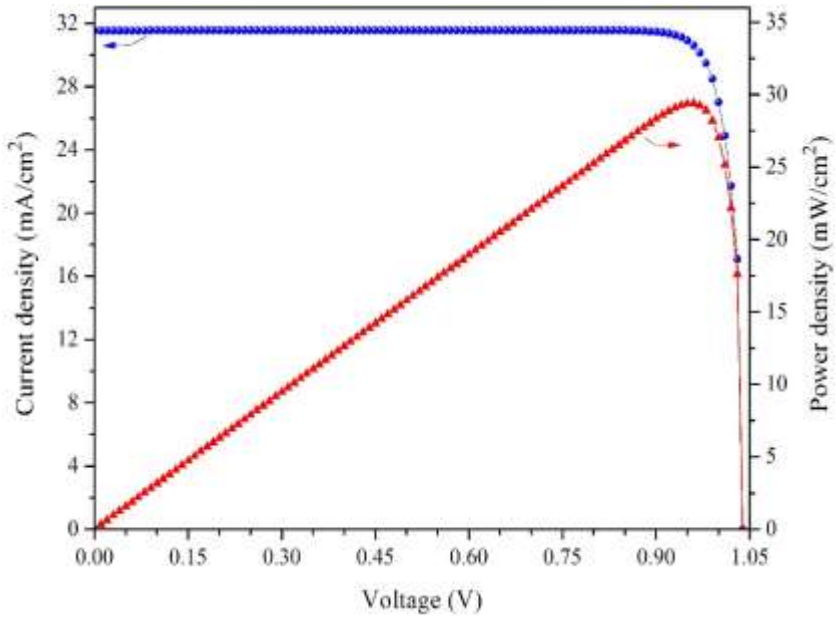

Fig. 5. $J(V)$ and $P(V)$ characteristics of the $In_{0.49}Ga_{0.51}P/GaAs$ top cell at T = 300 K.

5.2 Performance analysis of the Ge bottom sub-cell

Considering the part of the incident light that could not be absorbed by the heterojunction top cell, a bottom cell with a small bandgap energy is added to form a tandem structure capable to increase the total conversion efficiency. In particular, for this purpose, we considered a relatively thick substrate of *Ge* as in Fig. 1.

A first set of simulations has been performed to evaluate the performance of a single *Ge* solar cell. The fundamental geometrical and physical parameters used in (10)-(12) are listed in Table V [45,46]. In addition, the total thickness, i.e. y_4' in (11), is 150 μm and the depletion region edge in the p-*Ge* layer, i.e. y_3' in (11) and (12), is a value depending on both doping and bias level.

Table V. Physical and geometrical parameters for the *Ge* solar cell.

	Ge (n-type)	*Ge* (p-type)
y_1'(μm)	0.2	-
N_d (cm^{-3})	1×10^{16}-1×10^{19}	-
N_a (cm^{-3})	-	1×10^{18}
S_p (cm/s)	1×10^{5}-1×10^{6}	-
S_n (cm/s)	-	1×10^{6}

By fixing the physical parameters in the p-*Ge* base, different values of doping and recombination velocity of minority carriers in the n-*Ge* emitter are considered. A maximum conversion efficiency of 8.92% was obtained for $N_d = 2\times10^{18}$ cm^{-3} and $S_p = 10^5$ cm/s. Once again, an increased donor concentration affects both V_{oc} and J_{sc} as shown in Fig. 6.

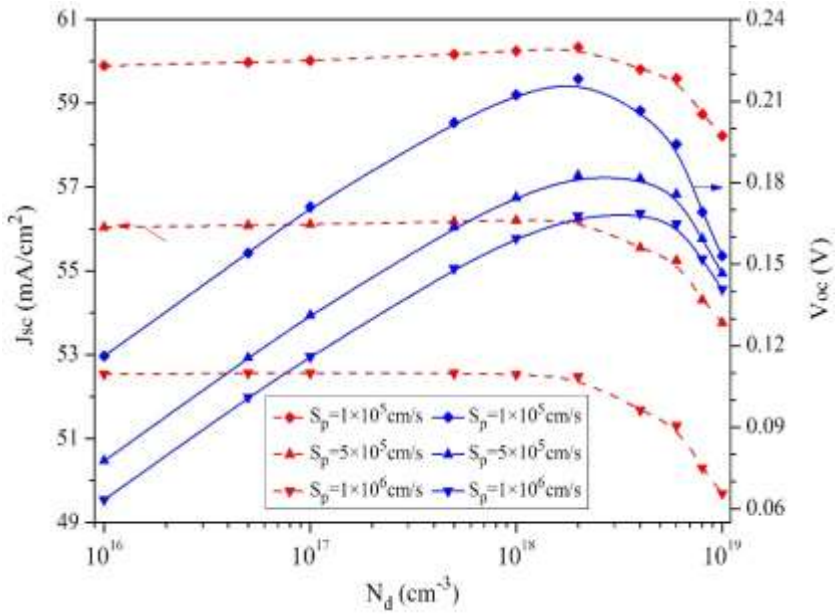

Fig. 6. J_{sc} and V_{oc} behaviors as a function of N_d and S_p for the single *Ge* solar cell.

The spectral response of the single *Ge* solar cell assuming $N_d = 2\times10^{18}$ cm^{-3} and $S_p = 1\times10^5$ cm/s in the emitter region, and $N_a = 1\times10^{18}$ cm^{-3} and $S_n = 1\times10^6$ cm/s in the base, is shown in Fig. 7. As can be seen, the cell responds to a wide part of the considered spectrum, and the spectral response exceeds 97% in the 0.9-1.4 μm wavelength range. Finally, the apparent *Ge*

bandgap energy, which is in the order of 0.63 eV, determines a cut-off wavelength close to 1.96 μm.

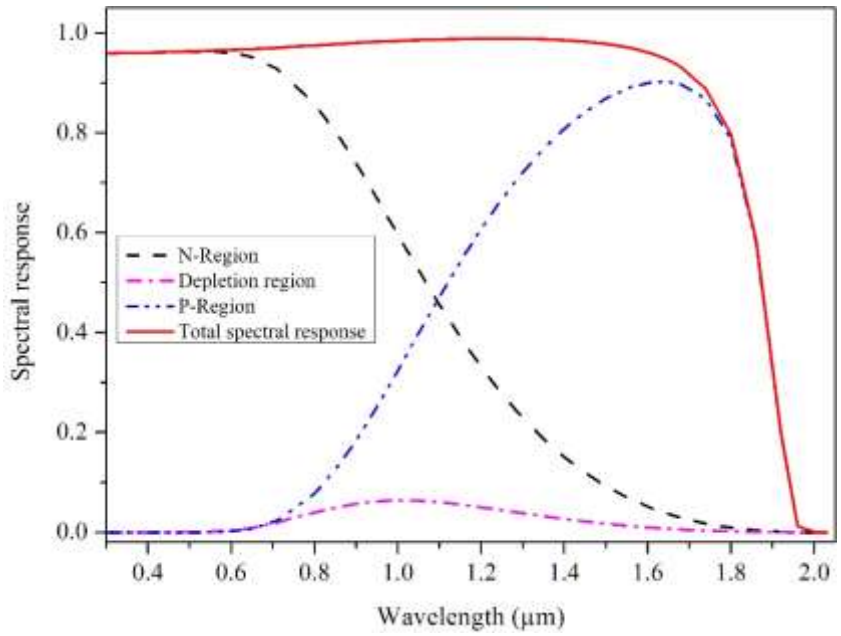

Fig. 7. Spectral response of the single *Ge* solar cell under AM1.5G spectrum.

By extracting the PV parameters from the $J(V)$ and $P(V)$ characteristics plotted in Fig. 8, we calculate J_{sc} = 60.34 mA/cm^2, V_{oc} = 0.22 V, P_{max} = 9.17 mW/cm^2, FF = 69.07% and $\eta_{300–2050}$ = 9.43%.

After this investigation, we have simulated and evaluated the performance of the *Ge* cell as bottom cell in the tandem structure. The short-circuit current density and open-circuit voltage behaviors as a function of the donor concentration and minority carrier recombination velocity assumed in the n-*Ge* emitter are shown in Fig. 9. For $N_d = 2\times10^{18}$ cm^{-3} and $S_p = 10^5$ cm/s, the maximum conversion efficiency is limited to 4.06%.

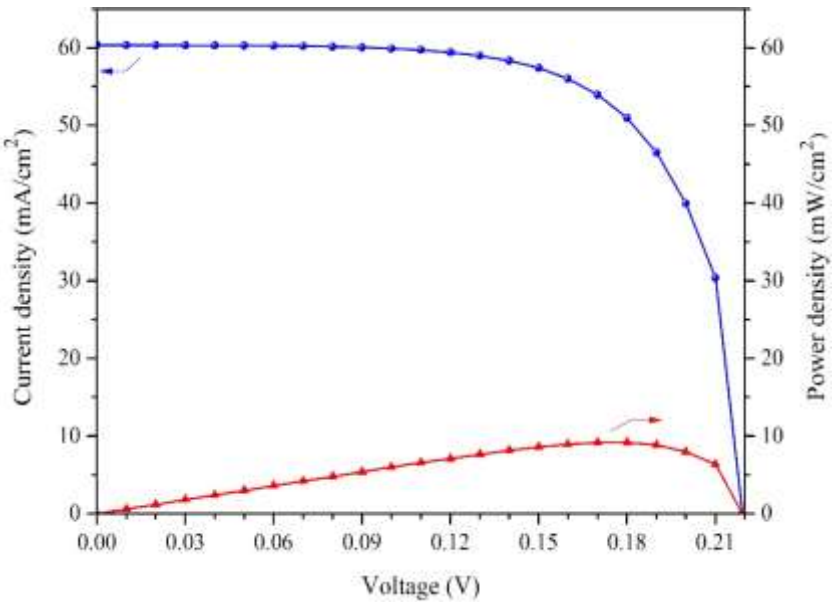

Fig. 8. $J(V)$ and $P(V)$ characteristics of a single *Ge* solar cell at $T = 300$ K.

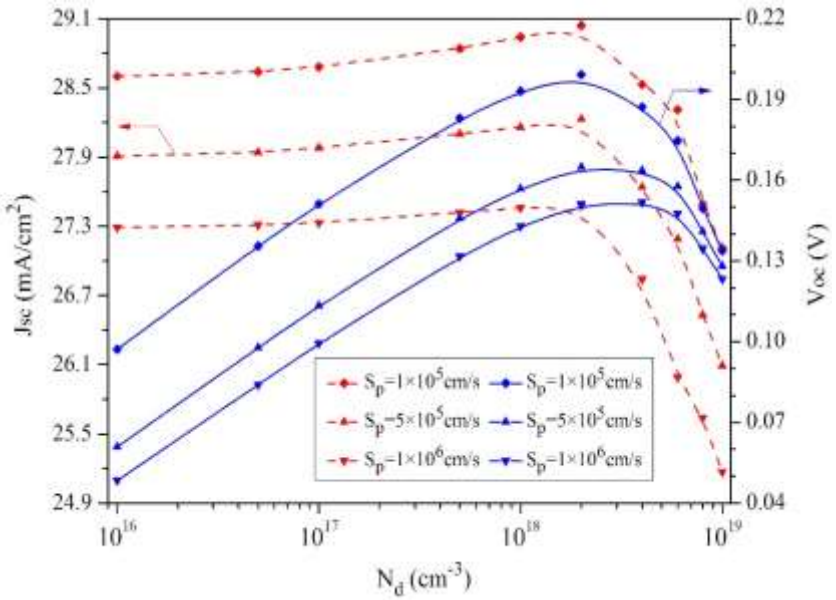

Fig. 9. J_{sc} and V_{oc} behaviors as a function of N_d and S_p for the *Ge* bottom cell in the tandem structure.

In this case, in fact, considering that the $In_{0.49}Ga_{0.51}P/GaAs$ top cell absorbs an important part of the incident spectrum as shown in Fig. 10, from the $J(V)$ and $P(V)$ characteristics plotted in Fig. 11 we calculate a lower performance of the *Ge* solar cell. In particular,

J_{sc} = 29.04 mAcm^{-2}, V_{oc} = 0.2 V, P_{max} = 3.95 mWcm^{-2}, FF = 68.01%, and $\eta_{300-2050}$ = 4.06% as mentioned above.

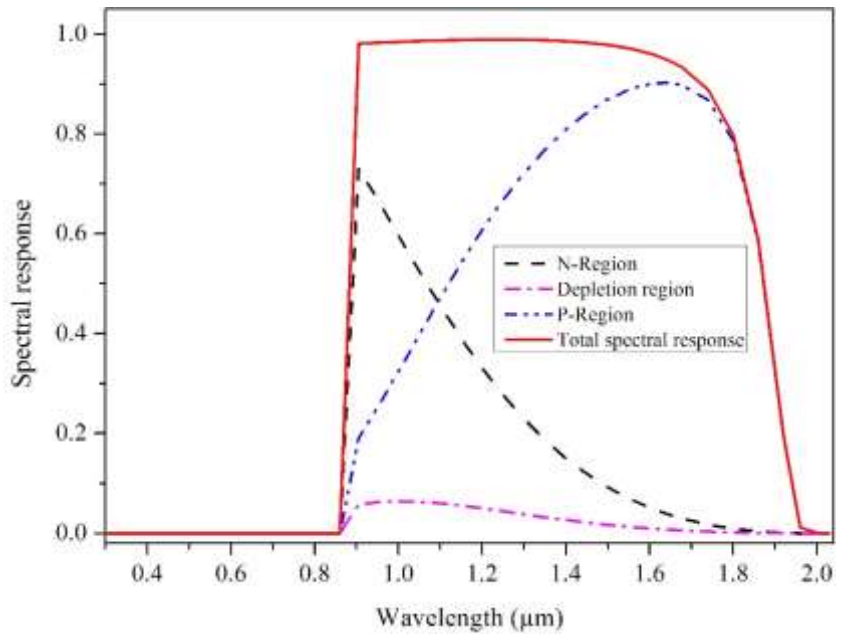

Fig. 10. Spectral response of the *Ge* bottom cell in the tandem structure under AM1.5G spectrum.

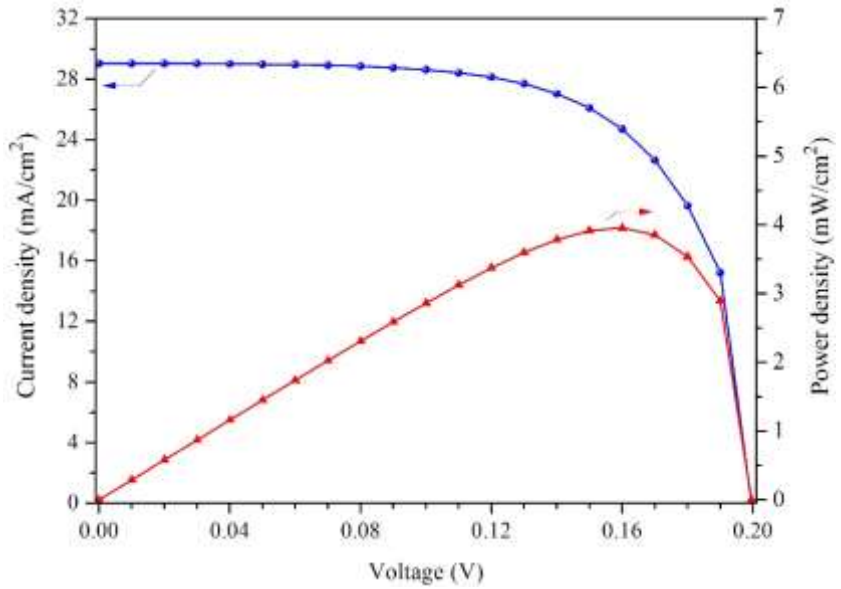

Fig. 11. $J(V)$ and $P(V)$ characteristics of the *Ge* bottom cell at T = 300 K.

5.3 Performance analysis of the $In_{0.49}Ga_{0.51}P/GaAs/Ge$ tandem cell

The spectral response and $J(V)$ curve of the tandem cell are shown in Figs. 12 and 13, respectively.

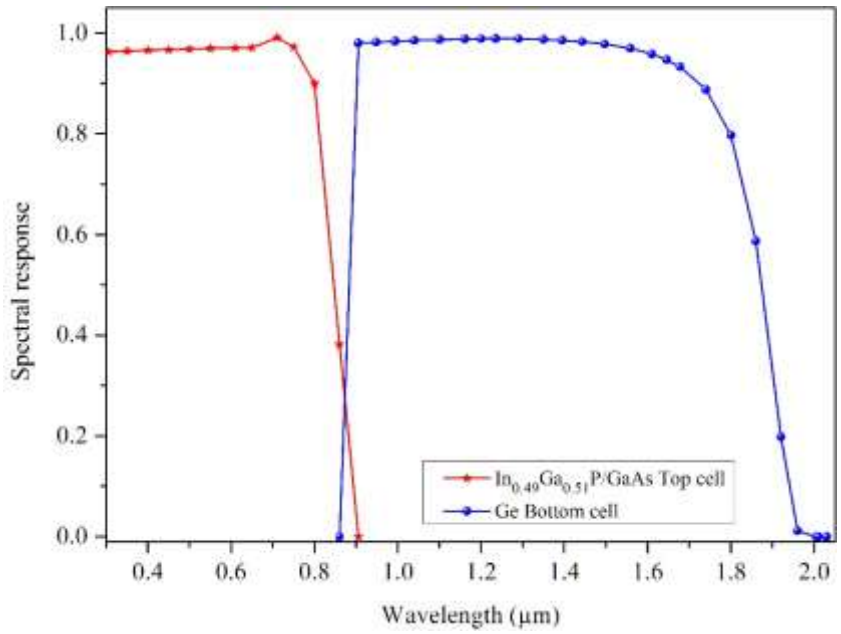

Fig. 12. Spectral response of the $In_{0.49}Ga_{0.51}P/GaAs/Ge$ tandem solar cell under AM1.5G spectrum.

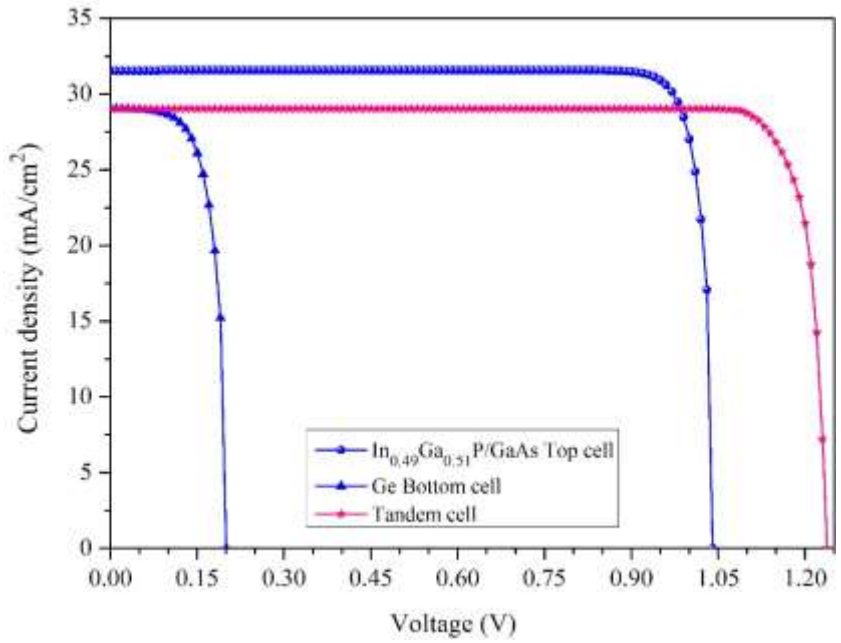

Fig. 13. $J(V)$ characteristics of the $In_{0.49}Ga_{0.51}P/GaAs$ top cell, *Ge* bottom cell, and tandem cell.

As expected, in Fig. 12 we can see a wide spectral response where the top cell responds to higher photon energy of shorter wavelengths, whereas the bottom cell responds to lower photon energy of longer wavelengths. At the same time, from Fig. 13, for the tandem structure the maximum value of the $J(V)$ curve is limited by the lower current density through the *Ge* cell considering that the two sub-cells are connected in series. On the other hand, the open-circuit voltage is the sum of the individual contributions.

The PV parameters extracted for the tandem cell are listed in Table VI. Here, the results obtained previously are also summarized for reader convenience.

Table VI. Photovoltaic parameters.

	V_{oc} (V)	J_{sc} (mA/cm^2)	P_{max} (mW/cm^2)	FF (%)	$\eta_{300-2050}$ (%)
Tandem cell	1.24	28.25	31.64	89.95	32.56
$In_{0.49}Ga_{0.51}P/GaAs$ top cell	1.04	31.55	29.38	89.54	30.24
G_e bottom cell	0.2	29.04	3.95	68.01	4.06
G_e single cell	0.22	60.34	9.17	69.07	9.43

The tandem cell maximum power density is 31.64 mW/cm^2. This value is calculated for a current density of 28.25 mA/cm^2 at a bias voltage of 1.12 V (see Fig. 13). The cell efficiency is 32.56%, namely a value lower than 5% of maximum efficiency that we could calculate for a 4-terminal device by adding, in principle, each sub-cell contribute (i.e., 30.24 + 4.06 = 34.3%).

Finally, experimental results for an InGaP/GaAs top cell mechanically stacked on a Ge-based bottom cell in a 2-terminal configuration are reported in Ref. 6, showing an overall conversion efficiency (non-optimized) in the limit of 16%.

5. Conclusions

In this work, using an analytical model, we have investigated the possibility to obtain a conversion efficiency in excess of 32.5% under AM1.5G spectrum for a dual-junction tandem

solar cell based on an $In_{0.49}Ga_{0.51}P/GaAs$ heterojunction top cell mechanically stacked on a *Ge* bottom cell.

In order to determine the device maximum overall conversion efficiency, the current density-voltage, power density-voltage, and spectral response behaviors have been calculated taking into account different values of fundamental physical parameters in the two sub-cell emitters. The obtained results seems to encourage the design of high efficiency dual junction tandem cells also considering the remarkable developments in the mechanical stack approach by means of transparent conductive adhesives.

References

[1] M. Baba, K. Makita, H. Mizuno, H. Takato, T. Sugaya, and N. Yamada, Prog. Photovolt. Res. Appl. 25, 255 (2017).

[2] R. M. France, P. Espinet-Gonzalez, N. J. Ekins-Daukes, H. Guthrey, M. A. Steiner, and J. F. Geisz, IEEE J. Photovolt. 8, 1608 (2018).

[3] S. Essig, S. Ward, M. A. Steiner, D. J. Friedman, J. F. Geisz, P. Stradins, and D. L. Young, Energy Procedia 77, 464 (2015).

[4] M. Schnabel, M. Rienäcker, E. L. Warren, J. F. Geisz, R. Peibst, P. Stradins, and A. C. Tamboli, IEEE J. Photovolt. 8, 1584 (2018).

[5] D. J. Friedman, Curr. Opin. Solid St. M. 14, 131 (2010).

[6] S. Yoshidomi, J. Furukawa, M. Hasumi, and T. Sameshima, Energy Procedia 60, 116 (2014).

[7] H. Bencherif, L. Dehimi, F. Pezzimenti, and F. G. Della Corte, Optik 182, 682 (2019).

[8] M. A. Green, K. Emery, Y. Hishikawa, W. Warta, E. D. Dunlop, D. H. Levi, and A. W. Y. Ho-Baillie, Prog. Photovolt: Res. Appl. 25, 3 (2017).

[9] B. M. Kayes, L. Zhang, R. Twist, I-K. Ding, and G. S. Higashi, IEEE J. Photovolt. 4, 729 (2014).

[10] B. Kınacı, Y. Özen, T. Asar, S. Ş. Çetin, T. Memmedli, M. Kasap, and S. Özçelik, J. Mater. Sci. Mater. Electron. 24, 3269 (2013).

[11] Y. Özen, N. Akın, B. Kınacı, and S. Özçelik, Sol. Energ. Mat. Sol. C. 137, 1 (2015).

[12] J. F. Geisz, M. A. Steiner, I. Garcia, S. R. Kurtz, and D. J. Friedman, Appl. Phys. Lett. 103, 041118 (2013).

[13] J. F. Wheelden, C. E. Valdivia, A. W. Walker, G. Kolhatkar, A. Jaouad, A. Turala, B. Riel, D. Masson, N. Puetz, S. Fafard, R. Ares, V. Aimez, T. J. Hall, and K. Hiazer, Prog. Photovoltaics 19, 442 (2011).

[14] P. T. Chiu, D. C Law, R. L. Woo, S. B. Singer, D. Bhusari, W. D. Hong, A. Zakaria, J. Boisvert, S. Mesropian, R. R. King, and N. H. Karam, in *IEEE 40th Photovoltaic Specialist Conference (PVSC) proceedings* (2014), pp. 11-13.

[15] J. W. Leem, Y. T. Lee, and J. S. Yu, Opt. Quant. Electron. 41, 605 (2009).

[16] S. Sato, H. Miyamoto, M. Imaizumi, K. Shimazaki, C. Morioka, K. Kawano, and T. Ohshima, Sol. Energy Mater. Sol. Cells 93, 768 (2009).

[17] R. R. King, D. C. Law, K. M. Edmondson, C. M. Fetzer, G. S. Kinsey, H. Yoon, R. A. Sherif, and N. H. Karam. Appl. Phys. Lett. 90, 183516 (2007).

[18] M. Lu, R. Wang, Y. Liu, Z. Feng, Z. Han, and C. Hou, Nucl. Instrum. Methods Phys. Res. B 307, 362 (2013).

[19] M. A. Green, M. J. Keevers, I. Thomas, J. B. Lasich, K. Emery, and R. R. King, Prog. Photovolt. Res. Appl. 23, 685 (2015).

[20] T. Sameshima, J. Takenezawa, M. Hasumi, T. Koida, T. Kaneko, M. Karasawa, and M. Kondo, Jpn. J. Appl. Phys. 50, 052301 (2011).

[21] L. Zhao, G. Flamand, and J. Poortmans, in *AIP conference proceedings of CPV-6 International Conference on Concentrating Photovoltaic System* (2010), pp. 284-289.

[22] T. P. White, N. N. Lal, and K. R. Catchpole, IEEE J. Photovolt. 4, 1 (2014).

[23] I. Mathews, D. O'Mahony, B. Corbett, and A. P. Morrison, Opt. Express 20, A754 (2012).

[24] S. M. Sze and K. K. Ng, Physics of Semiconductor Devices, 3rd edn, (J. Wiley & Sons, New York, 2006), p. 790.

[25] K. Zeghdar, L. Dehimi, F. Pezzimenti, S. Rao, and F. G. Della Corte, Jpn. J. Appl. Phys. 58, 014002 (2019).

[26] F. G. Della Corte, F. Pezzimenti, S. Bellone, and R. Nipoti, Mater. Sci. Forum 679, 621 (2011).

[27] F. Pezzimenti, IEEE Trans. Electron Dev. 60, 1404 (2013).

[28] M. Y. Ghannam, A. S. Al Omar, N. Posthuma, G. Flammand, and J. Poortmans, Kuwait J. Sci. Eng. 3, 203 (2004).

[29] S. C. Jain and D.J. Roulston, Solid-State Electron. 34, 453 (1991).

[30] A. W. Haas, J. R. Wilcox, J. L. Gray, and R. J. Schwartz, J. Photon. Energy 1, 018001 (2011).
[31] M. L. Megherbi, F. Pezzimenti, L. Dehimi, M. A. Saadoune, and F. G. Della Corte, IEEE Trans. Electron Dev. 65, 3371 (2018).
[32] F. Pezzimenti and F. G. Della Corte, in *Mediterranean Electrotechnical Conference proceedings - MELECON* (2010), pp. 1129-1134.
[33] M. L. Megherbi, F. Pezzimenti, L. Dehimi, A. Saadoune, and F. G. Della Corte, J. Electron. Mater. 47, 1414 (2018).
[34] M. Sotoodeh, A. H. Khalid, and A. A. Rezazadeh, J. Appl. Phys. 87, 2890 (2000).
[35] D. B. M. Klaassen, Solid-State Electron. 35, 961 (1992).
[36] P. T. Landsberg, and G. S. Kousik, J. Appl. Phys. 56, 1696 (1984).
[37] F. Bouzid and N. Benaziez, Int. J. Renew. Energy Res. 4, 759 (2014).
[38] G. De Martino, F. Pezzimenti, F. G. Della Corte, G. Adinolfi, and G. Graditi, in *IEEE proceedings of Int. Conf. Ph. D. Research in Microelectronics and Electronics - PRIME* (2017), pp. 221-224.
[39] F. Bouzid, L. Dehimi, and F. Pezzimenti, J. Electron Mater. 46, 6563 (2017).
[40] Y. Marouf, L. Dehimi, F. Bouzid, F. Pezzimenti, F. G. Della Corte, Optik 163, 22 (2018).
[41] F. Bouzid, F. Pezzimenti, L. Dehimi, M. L. Megherbi, and F. G. Della Corte, Jpn. J. Appl. Phys. 56, 094301 (2017).
[42] F. G. Della Corte, G. De Martino, F. Pezzimenti, G. Adinolfi, G. Graditi, IEEE Trans. Electron Dev. 68, 3352 (2018).
[43] F. Bouzid, L. Dehimi, F. Pezzimenti, M. Hadjab, and A.H. Larbi, Superlattice. Microst. 122, 57 (2018).
[44] S. R. Kurtz, J. M. Olson, D. J. Friedman, J. F. Geisz, K. A. Bertness, and A. E. Kibbler, in *Compound Semiconductor Surface Passivation and Novel Device, MRS Proceedings* (1999), pp. 1-15.
[45] A. S. Gudovskikh, K. S. Zelentsov, N. A. Kalyuzhnyy, V. M. Lantratov, S. A. Mintairov, and J. P. Kleider, Energy Procedia 3, 76 (2011).
[46] T. Wilson, T. Thomas, M. Führer, N. J. Ekins-Daukes, R. Roucka, A. Clark, A. Johnson, R. Hoffman Jnr., and D. Begarney, in *AIP conference proceedings of CPV-12 International Conference on Concentrating Photovoltaic System* (2016), pp. 1-6.

Figure captions

Fig.1. Simulated $In_{0.49}Ga_{0.51}P/GaAs/Ge$ dual-junction tandem solar cell (2-terminal device).

Fig. 2. Conversion efficiency of the $In_{0.49}Ga_{0.51}P/GaAs$ top cell as a function of N_d and S_p at $T = 300$ K.

Fig. 3. J_{sc} and V_{oc} behaviors as a function of N_d and S_p for the $In_{0.49}Ga_{0.51}P/GaAs$ top cell.

Fig. 4. Spectral response of the $In_{0.49}Ga_{0.51}P/GaAs$ top cell under AM1.5G spectrum.

Fig. 5. $J(V)$ and $P(V)$ characteristics of the $In_{0.49}Ga_{0.51}P/GaAs$ top cell at $T = 300$ K.

Fig. 6. J_{sc} and V_{oc} behaviors as a function of N_d and S_p for the single *Ge* solar cell.

Fig. 7. Spectral response of the single *Ge* solar cell under AM1.5G spectrum.

Fig. 8. $J(V)$ and $P(V)$ characteristics of a single *Ge* solar cell at $T = 300$ K.

Fig. 9. J_{sc} and V_{oc} behaviors as a function of N_d and S_p for the *Ge* bottom cell in the tandem structure.

Fig. 10. Spectral response of the *Ge* bottom cell in the tandem structure under AM1.5G spectrum.

Fig. 11. $J(V)$ and $P(V)$ characteristics of the *Ge* bottom cell at $T = 300$ K.

Fig. 12. Spectral response of the $In_{0.49}Ga_{0.51}P/GaAs/Ge$ tandem solar cell under AM1.5G spectrum.

Fig. 13. $J(V)$ characteristics of the $In_{0.49}Ga_{0.51}P/GaAs$ top cell, *Ge* bottom cell, and tandem cell.